Dysregulation of Autophagy Occurs During Congenital Cataract Development in βA3ΔG91 Mice

Akosua K. Boateng, Roy Joseph, and Om P. Srivastava

Department of Optometry and Vision Science, School of Optometry, University of Alabama at Birmingham, Birmingham, Alabama, United States

Correspondence: Om P. Srivastava, Department of Optometry and Vision Science, School of Optometry, University of Alabama at Birmingham, 1025 18th Street South, Birmingham, AL 35294, USA; srivasta@uab.edu.

OPS is the senior author.

Received: July 25, 2023
Accepted: February 27, 2024
Published: April 1, 2024

Citation: Boateng AK, Joseph R, Srivastava OP. Dysregulation of autophagy occurs during congenital cataract development in βA3ΔG91 mice. *Invest Ophthalmol Vis Sci.* 2024;65(4):4. https://doi.org/10.1167/iovs.65.4.4

Purpose. To examine lens phenotypic characteristics in βA3ΔG91 mice and determine if βA3ΔG91 affects autophagy in the lens.

Methods. We generated a βA3ΔG91 mouse model using CRISPR/Cas9 methodology. Comparative phenotypic and biochemical characterizations of lenses from postnatal day 0 (P0), P15, and 1-month-old βA3ΔG91 and wild-type (WT) mice were performed. The methodologies used included non-invasive slit-lamp examination, reverse transcription–quantitative polymerase chain reaction (RT-qPCR), western blot, and immunohistochemical (IHC) analyses to determine the levels of autophagy-related genes and proteins. Transmission electron microscopy (TEM) analysis of lenses was performed to assess organelle degradation and the presence of autophagic vesicles. TUNEL staining was used to determine apoptosis in the lens.

Results. Relative to WT lenses, 1-month-old βA3ΔG91 mice developed congenital nuclear cataract and microphthalmia and showed an early loss of endoplasmic reticulum (ER) in the cortex and attenuation of nuclei degradation. This observation was confirmed by TEM analysis, as was the presence of autophagic vesicles in βA3ΔG91 lenses. Comparative IHC and RT-qPCR analyses showed relatively higher levels of autophagy markers (ubiquitinated proteins and p62, LC3, and LAMP2 proteins) in βA3ΔG91 lenses compared to WT lenses. Additionally, βA3ΔG91 lenses showed relatively greater numbers of apoptotic cells and higher levels of cleaved caspase-3 and caspase-9.

Conclusions. The deletion of G91 in βA3ΔG91 mice leads to higher levels of expression of autophagy-related proteins and their transcripts relative to WT lenses. Taken together, G91 deletion in βA3/A1-crystallin is associated with autophagy disruption, attenuation of nuclei degradation, and cellular apoptosis in the lens, which might be congenital cataract causative factors.

Keywords: βA3/A1-crystallin, congenital cataract, autophagy, lens

The crystalline lens is composed of a single layer of lens epithelial cells (LECs) that differentiate at the equator into lens fiber cells throughout life to maintain lens transparency.[1] During the differentiation of epithelial cells to fiber cells, transitioning lens epithelial cells undergo programmed degradation of organelles to produce an organelle-free zone (OFZ).[2,3] Autophagy is a major cellular event involved in the clearance of organelles as well as misfolded or aggregated proteins in the lens,[4–6] and impairment of this process could result in cataract formation.[7,8]

Congenital cataracts cause approximately 10% of childhood blindness worldwide, occurring at a rate of three to six per 10,000 live births worldwide[9] and three to four visually significant cataracts per 10,000 live births in the United States.[10] Heterogeneous congenital cataracts, inherited as autosomal recessive, autosomal dominant, or X-linked traits, represent ~8% to 25% of non-syndromic cataracts.[9] Approximately one-third of pediatric cataract mutations are hereditary,[11] and among these mutations, ~50% are found in crystallins, ~25% in connexins, and the remainder in other structural genes and transcription factors.[12] Several mutations in βA3/A1-crystallin have been identified that cause autosomal-dominant congenital cataracts,[12] most of which are clustered at two sites; one occurs at the exon 3 splice site and the other is an exon 4 in-frame deletion.[13–23] Among the CRYβA1 mutations, one common βA3ΔG91 mutation has been shown to cause congenital nuclear cataract in several ethnically disparate families.[13,16–22,24]

In vertebrates, crystallins are classified as α-, β-, or γ-crystallins. Even though these crystallins have been studied extensively, β-crystallins remain elusive in their structural significance and functions. This is partly because of the existence of their several subunits and tendency to form oligomers.[25] β-crystallins are further subdivided into three basic (βB-) and four acidic (βA-) proteins.[25,26] Of all β-crystallins, βA3/A1-crystallin remains a unique lens structural protein because it produces two protein isoforms (βA1- and βA3-crystallins) from a single *CRYβA1* mRNA via an alternative translation initiation site by leaky ribosomal scanning.[27] The two proteins share sequence homology except that βA1-crystallin is 17 amino acids shorter at the N-terminal region than βA3-crystallin.[27] Structurally, βA3/

A1-crystallin is encoded by six exons, out of which four (exons 3–6) code for four Greek key motifs that fold into two similar domains, connected by a short peptide.[27] The distinctive Greek key pattern of β- and γ-crystallins is required to maintain lens transparency and the refractive power of the lens.[28]

In rodents, βA3/A1-crystallin mRNA is first detected around embryonic day 12.5 in the posterior lens vesicle, suggesting its role in early lens development.[29] Despite a robust expression in the lens, βA3/A1-crystallin is also expressed in the retinal pigment epithelium (RPE), retinal astrocytes, and the brain.[29–32] Although the function of βA3/A1-crystallin as a lysosomal resident protein and an autophagy regulator is well studied in the retina,[30–32] its similar function in the lens, other than as a structural protein, remains unclear. Interestingly, studies have shown that an absence of βA3/A1-crystallin in murine lenses leads to autophagy disruption and cataract development.[31–34]

Among the βA3/A1-crystallin mutations that cause human congenital cataracts, there is the commonly occurring in-frame deletion of a highly conserved Gly-91 within the second Greek key motif (βA3ΔG91). This autosomal dominant congenital nuclear cataract, discovered in several ethnically disparate families worldwide, causes a dysfunctional βA3/A1-crystallin due to the loss of its structural integrity. It is evidenced by the recombinant G91-deleted βA3/A1-crystallin, which has shown defective refolding, loss of solubility, and oligomerization with other crystallins.[19,35] In order to explore the molecular mechanism of βA3ΔG91-induced congenital cataract, we have generated a βA3ΔG91 knock-in mouse model using CRISPR/Cas9 methodology. Here, we report comparative phenotypic characteristics of lenses of βA3ΔG91 mice and wild-type (WT) mice and show that the mutation leads to the disruption of autophagy. Our mutant mice showed nuclei and mitochondria being retained in the OFZ and exhibited elevated levels of autophagy markers and cellular apoptosis relative to WT mice. This finding strongly suggests that autophagy is associated with cataract development of βA3ΔG91 mice lenses relative to WT mice lenses.

Materials and Methods

Ethics Statement

All animal experiments were conducted in accordance with protocols approved by the Institutional Animal Care and Use Committee (IACUC) of the University of Alabama (UAB) at Birmingham (protocol no. 08393), and all procedures adhered to the ARVO Statement for the Use of Animals in Ophthalmic and Vision Research. Mice were kept under a 12-hour/12-hour light/dark cycle in a controlled, pathogen-free facility of the University of Alabama at Birmingham.

Generation of βA3ΔG91 Mice

The βA3ΔG91 mouse model was generated at the UAB Transgenic and Genetically Engineered Models (TGEMs) Core Facility using CRISPR/Cas9 methodology. Briefly, a CRISPR guide RNA was designed using CRISPOR.tefor.net to target exon 4 on the mouse Cryba1 locus adjacent to Gly-91. A symmetrical 200-bp single-stranded DNA (ssDNA) repair template was designed to introduce the desired mutation, as well as an additional silent mutation creating a second Taq1-restriction site for genotyping. The CRISPR guide RNA and Cas9 protein were complexed in vitro before injection at a concentration of 50-ng/μL guide RNA, 50-ng/μL Cas9 protein, and 50-ng/μL ssDNA repair template into 0.5-day mouse embryos. Embryos surviving microinjection were transferred into pseudo-pregnant C57BL/6 recipient mice to develop to term. Desired timed-mating was performed between female C57BL/6 mice and male founder βA3ΔG91 mice to generate autosomal-dominant βA3ΔG91 mice. All mice were bred in a C57BL/6 strain background.

PCR and DNA Analysis

Genomic DNA was extracted from mouse tail tissues using a DNA isolation kit from QIAGEN (Germantown, MD, USA). For initial verification of the knock-in, PCR products were sequenced in the UAB Heflin Center for Genomic Sciences. PCR primers used for genotyping were βA3ΔG91 (forward: 5′-AGGTCTTCTCCCTTAGGCCA-3′) and βA3ΔG91 (reverse: 5′-ACTAGAAGAGGGCACGGGAT-3′). Following PCR amplification, the restriction enzyme digestion was performed using Taq1-v2 endonuclease (New England Biolabs, Ipswich, MA, USA), and analyzed by using a 6% polyacrylamide gel.

Lens Imaging

The lenses from postnatal day 0 (P0), P15, and P30 βA3ΔG91 and WT mice were enucleated and imaged using a microscope with a charge-coupled device (CCD) camera attachment. One-month-old βA3ΔG91 and WT mice were subjected to minimal anesthesia containing a ketamine–xylazine cocktail (0.05 mL/20g mouse weight, by intraperitoneal injection). Their eyes were dilated with 0.5% tropicamide eye drops and were examined within 5 minutes with a hand-held slit-lamp biomicroscope equipped with a camera.

PCR Analyses

RNA was extracted from mice lenses ($n = 6$ from WT and βA3ΔG91 mice) using the TRIzol method, and 1 μg of total RNA from each lens was reverse transcribed using an Invitrogen cDNA Synthesis Kit (Thermo Fisher Scientific, Waltham, MA, USA). The housekeeping gene glyceraldehyde 3-phosphate dehydrogenase (*GAPDH*) served as an endogenous control for the quantitation of autophagy-related genes. Primers used in the reverse transcription–quantitative polymerase chain reaction (RT-qPCR) analyses are listed in Table 1.

Protein Extraction and Mass Spectrometry Analyses

Lens proteins were extracted from WT and βA3ΔG91 mice and separated into water-soluble (WS), water-

Table 1. Primer Sequences for QPCR Analyses

Primers	Primer Sequences (5′–3′)
LC3B	Forward: 5′-ATCCCAGTAGGTTCTCCTGC-3′
	Reverse: 5′-CGCTCTATAATCACCCGCC-3′
p62	Forward:5′-GGACCCATCTACAGAGGCTG-3′
	Reverse: 5′-ACTGGATCGTGTCCAGAGCA-3′
LAMP2	Forward: 5′-GGACAGTATTCTACAGCCCAGGAG-3′
	Reverse: 5′-CCAGCATAGGTCTTTCTTCTGCC-3′
CRYβA1	Forward: 5′-TGGAGTGTGGCGCAATCATA-3′
	Reverse: 5′-GAAGTCTGGGCGTGAGATCC-3′

Table 2. Mass Spectrometric Analyses: Normalized Spectral Counts* for CRYβA1/A3 in WT Versus βA3ΔG91 Lenses

	WT	βA3ΔG91	Difference (βA3ΔG91 – WT)
Water-soluble	17.29	7.45	−9.84
Water-insoluble–urea-soluble	9.23	6.19	−3.05
Water-insoluble–urea-insoluble	2.72	6.70	3.98

* As described in the Materials and Methods section.

insoluble–urea-soluble (WI-US), and water-insoluble–urea-insoluble (WI-UI) fractions, following previously described methods.[52] Protein concentrations in these fractions were determined using the Pierce BCA Protein Assay Kit (Thermo Fisher Scientific). Lens proteins were electrophoretically separated by SDS-PAGE using 12% polyacrylamide gels. Following mass spectrometry (MS) analyses,[52] with a confidence score set to at least 95%, spectral counts were computed by summing the number of MS/MS identifications for βA3/A1-crystallin. Spectrum count normalization in Scaffold was used (Proteome Software, Portland, OR, USA). Briefly, the normalized spectral count for βA3/A1-crystallin was calculated as $spectrum\ \ count * \frac{average\ spectral\ count\ between\ WT\ and\ \beta A3\Delta G91}{total\ spectral\ count\ per\ group}$. Normalized spectral counts for βA3/A1-crystallin are listed in Table 2.

Immunoblotting

Isolated lenses ($n = 6$, from WT and βA3ΔG91 mice) were homogenized in radioimmunoprecipitation assay (RIPA) buffer (Sigma-Aldrich, St. Louis, MO, USA) containing a protease inhibitor cocktail tablet (Roche, Indianapolis, IN, USA). Protein concentration was measured using a BCA Protein Assay Kit. Between 50 and 80 µg of lens protein was electrophoretically separated using 12% polyacrylamide gels, and the protein bands were transferred to a polyvinylidene fluoride (PVDF) membrane (Bio-Rad, Hercules, CA, USA). The blots were blocked with 5% non-fat dry milk in TBS for 1 hour and incubated with primary antibodies (LC3, anti-βA3-crystallin) at 4°C overnight. After three washes with TBST (Tris-buffered saline + 0.1% Tween 20), blots were incubated with a secondary IRDye 800CW antibody, and protein bands were visualized using LI-COR Odyssey system (LI-COR, Lincoln, NE, USA). GAPDH was used as the loading control (Cell Signaling Technology, Danvers, MA, USA). Full images of immunoblots are provided in the Supplementary Figures.

Histology and Immunofluorescence

Eyes from P0, P15, and 1-month-old βA3ΔG91 and WT mice were enucleated and immediately embedded in Tissue-Tek O.C.T compound (Sakura Finetek USA, Torrance, CA, USA). They were kept on dry ice for 1 hour and then transferred to −80°C. Eyes were then cut into 16-µm sections using a Leica cryostat (Leica Biosystems, Deer Park, IL, USA). Lens sections were fixed in 4% paraformaldehyde (PFA) for 10 minutes. For all immunofluorescence studies, the sections were blocked in 5% goat serum and 1% BSA in PBS for 1 hour and incubated overnight with a desired primary antibody. The primary antibodies used in this study included anti-βA3-crystallin (ab151722; Abcam, Waltham, MA, USA); anti-p62/SQSTM (55274-I-AP; Proteintech, Rosemont, IL, USA); anti-ubiquitin (58395S; Cell Signaling Technology); anti-LC3 (A17424; Cell Signaling Technology); anti-LAMP2 (66301-1-Ig; Proteintech); anti-cleaved caspase-3 (9664; Cell Signaling Technology); and anti-cleaved caspase-9 (9507; Cell Signaling Technology). The sections were washed with PBS and incubated with fluorophore-labeled secondary antibodies (Thermo Fisher Scientific) for 1 hour in the dark at room temperature. The lens tissues were washed in phosphate-buffered saline with 0.1% Tween 20 (PBST) and counterstained with Hoechst 33342 or 4′,6-diamidino-2-phenylindole (DAPI)-containing mounting medium. Photographs were taken with a Nikon AX-R laser confocal microscope (Nikon, Tokyo, Japan) or, in some cases, with a Zeiss Axioplan 2 fluorescence microscope equipped with a CCD camera (Carl Zeiss Microscopy, Jena, Germany) at the UAB Vision Science Research Center core facility. Signal intensities were quantified using Image J (National Institutes of Health, Bethesda, MD, USA).

Cell Culture Studies

Lens epithelial cells from WT and βA3ΔG91 mice were cultured as previously described.[33] Briefly, lenses from 4- to 5-week-old mice were extracted and incubated in 0.25% trypsin for 3 hours. Cells were then recovered by centrifuging at 1500 rpm and cultured in M199 medium containing 2% fetal bovine serum (HyClone, Logan, UT, USA). For all immunofluorescence studies, cells were plated on eight-well chambered slides. The immunostaining procedure was performed as described above. To induce autophagy in vitro, lens epithelial cells from WT and βA3ΔG91 mice were serum starved for 18 hours. In the same way, autophagy inhibition was carried out by treating cells with bafilomycin A1 (100 nM) for 18 hours.

Transmission Electron Microscopy

Lenses from 1-month-old WT and βA3ΔG91 mice were fixed in a modified Karnovsky's fixative (2% PFA with 2% glutaraldehyde in 0.1-M phosphate buffer; Microscopy Science, Hatfield, PA, USA) for 1 hour at room temperature and then kept at 4°C overnight. The fixed lenses were rinsed several times with 0.1-M sodium cacodylate buffer (pH 7.4) and post-fixed with 1% OsO_4 in cacodylate buffer for 1 hour in the dark. After several rinses in cacodylate buffer, lenses were dehydrated through a series of graded 50% to 100% ethyl alcohol. Next, the tissues were placed in a 1:1 mixture of propylene oxide and embedding resin overnight. The following day, the lenses were transferred into a fresh change of 100% embedding media and left overnight to polymerize in a 60°C embedding oven. Ultra-thin sections (70- to 80-nm thickness) were cut using a Leica Ultracut UCT 7 ultramicrotome and stained with uranyl acetate and lead citrate. The lens sections were imaged on an FEI 120 kv Spirit TEM (FEI Company, Hillsboro, OR, USA), and images were collected using a BioSprint 29 CCD camera (AMT Imaging, Woburn, MA, USA).

Apoptosis Assay

Apoptotic cells in lens tissues were detected using a Roche Fluorescein In Situ Cell Death Detection Kit. TUNEL staining was performed according to the manufacturer's protocol, and fluorescent images of the sections were taken with a Zeiss Axioplan 2 fluorescence microscope equipped with a CCD camera.

Statistical Analysis

Data were recorded as mean ± SD, and analyzed using R 4.0.5 for Windows (R Foundation for Statistical Computing, Vienna, Austria). Significant differences were evaluated by analysis of independent Student's *t*-test (two-tailed). Statistical significance was defined as $P < 0.05$. All experiments were performed and repeated in triplicate.

Results

Generation and Characterization of βA3ΔG91 Mice

CRISPR/Cas 9 technology was used to generate the βA3ΔG91 knock-in mouse model. The knock-in mutation was verified via DNA sequencing, which confirmed the 3-bp (GAG) deletion that resulted in the deletion of Gly-91 in F0 founder mice, as shown by dashes highlighted in pink in Figure 1A. In these mice, an additional silent mutation was introduced to induce a second TˆCGA site (Fig. 1A, black arrowhead), in addition to the first (black arrow), which is originally present in the genome. The TˆCGA sequence is recognized and cleaved by the Taq1 endonuclease, producing three nucleotide fragments in βA3ΔG91 mice instead of two fragments in the WT mice during genotyping (Fig. 1B). After successfully generating the mouse model, we used the hand-held slit lamp to examine 1-month-old mice for cataract development. βA3ΔG91 mice exhibited a dense nuclear cataract and microphthalmia (Fig. 1C, right panel) compared to lenses of WT mice (Fig. 1C, left panel). Upon gross inspection, the anterior chamber and ocular adnexa appeared normal. Whole lens tissues and LECs were extracted from 1-month-old WT and βA3ΔG91

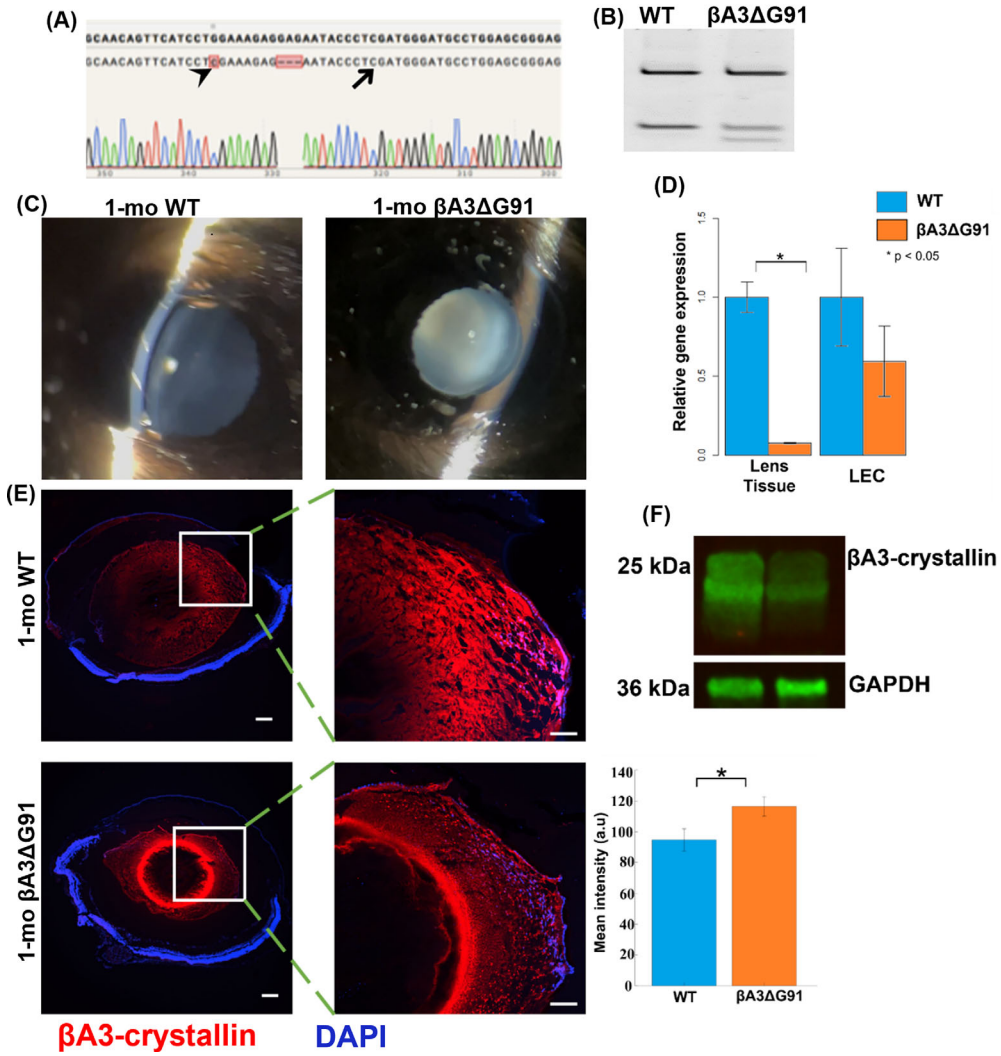

Figure 1. Phenotypic characterization of βA3ΔG91 mice. (**A**) DNA from the tail was amplified with primers spanning the target region on exon 4 of the *CRYβA1/A3* gene. Sequence analysis verifies the GAG deletion that leads to the glycine-91 deletion and the additional silent mutation, creating a second TaqI restriction site for genotyping (*black arrowhead*). (**B**) Genotyping results show two and three bands for WT and βA3ΔG91 mice, respectively. (**C**) Slit-lamp photographs of 1-month-old mice revealed that the mutant mice had a dense nuclear cataract (*right*) whereas the WT mice had a clear lens. (**D**) Significantly lower levels of *CRYβA1* mRNA seen in the whole lens tissue is demonstrated by RT-qPCR analysis (*left graph*). (**E**) IHC revealed a relatively smaller lens with puncta in the outer cortex, and a bright ring-like pattern formed in the inner cortex of βA3ΔG91 lenses (shown in 4× and 20×, respectively). *Scale bar*: 200 µm. *$P < 0.05$ versus age-matched WT. (**F**) Western blots of RIPA-soluble lens homogenates probed with the anti-βA3-crystallin antibody show a decreased expression of the protein in βA3ΔG91 lenses relative to WT lenses. GAPDH was used as a loading control.

Investigative Ophthalmology & Visual Science

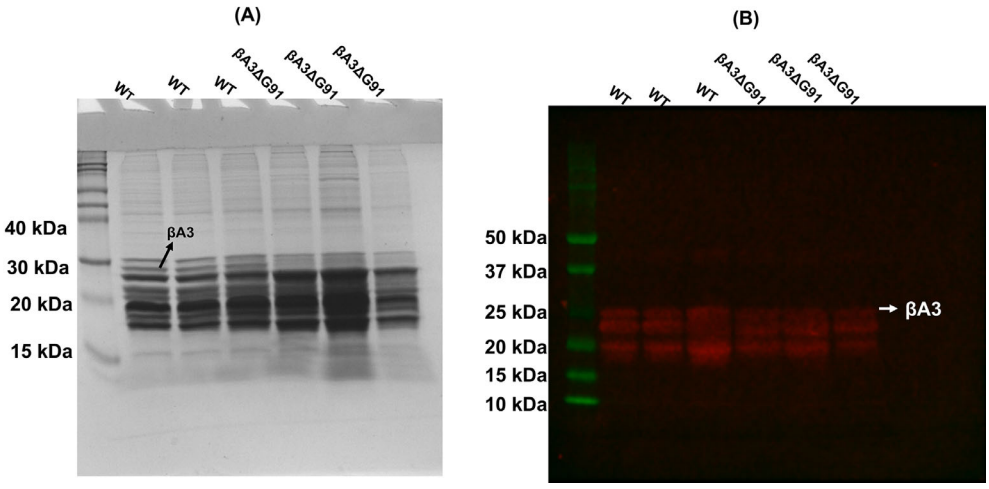

Figure 2. Coomassie blue staining and western blot analysis of RIPA buffer–solubilized proteins from lenses of WT and βA3ΔG91 mice. (**A**) Three individual lenses from both types of mice were solubilized in identical volumes of RIPA buffer, and identical volumes of the preparations were analyzed by SDS-PAGE using 12% polyacrylamide gels. (**B**) During western blot analysis, the anti-βA3 antibody (see Fig. 1F) was utilized.

mice to determine *CRYβA1* gene expression by RT-qPCR (Fig. 1D). In the whole lens tissue, *CRYβA1* mRNA was significantly downregulated in βA3ΔG91 lenses compared to the WT lenses. Additionally, our immunohistochemical (IHC) analyses using anti-βA3-crystallin antibody showed punctate staining in the outer cortex and a bright ring-like pattern in the inner cortex of the mutant lens sections (Fig. 1E, lower panel), which was not present in the WT lenses (Fig. 1E, upper panel). Interestingly, immunoblots of the RIPA-soluble lens protein fractions corroborated our qPCR studies by showing decreased levels of βA3/A1-crystallin expression in βA3ΔG91 lenses relative to the WT lenses (Fig. 1F). The βA3-crystallin immunoreactive ring-structure during IHC (Fig. 1E, lower panel) suggested the possibility that βA3ΔG91 protein becomes water insoluble in the cortex, and it causes the protein to accumulate in the form of a ring (perhaps at the outer edge of nuclear cataract), which was absent in the WT lenses. This was supported by the insolubility of recombinant βA3ΔG91 protein as described in a previous report.[19] Further, we speculate that the intense ring in the nuclear region of βA3ΔG91 lenses compared to the WT lenses (Fig. 1E) could represent insolubilization of the crystallin and could be a cataractogenic factor. As described above, the western blot analysis with anti-βA3-crystallin antibody of the soluble fraction showed that the immunoreactive βA3-crystallin band was found to be at relatively lower levels compared to the lenses from WT mice (Fig. 1F). We suspected that the decreased expression of βA3-crystallin in our western blot was due to either degradation or insolubilization or both of the crystallin in βA3ΔG91 lenses relative to WT lenses. To further examine this, we comparatively analyzed the WS and WI protein fractions of the two types of lenses by western blot analysis and mass spectrometry. As shown in Fig. 2A, the Coomassie-blue–stained gel protein profiles of the RIPA buffer-soluble proteins showed the loss of a 25-kDa βA3 crystallin band in βA3ΔG91 lenses relative to WT lenses (identified by an arrow). On western blot analysis with the same anti-βA3 crystallin antibody as used in Figure 1F, the level of the immunoreactive band of 25 kDa was relatively reduced in βA3ΔG91 lenses relative to WT lenses (identified by an arrow in Fig. 2B). Additionally, the comparative mass spectrometric analyses of WS, WI-US, and WI-UI proteins of 1-month-old βA3ΔG91 and WT mice showed that, relative to WT lenses, βA3ΔG91 lenses exhibited relatively greater levels of insolubility of βA3-crystallin in WI-UI protein fractions (Table 2). Together, the data suggest that βA3-crystallin undergoes both degradation and insolubilization in βA3ΔG91 lenses relative to WT lenses.

Delayed Nuclei Degradation in Lenses of βA3ΔG91 Mice Relative to WT Mice

Following epithelial to fiber cell differentiation, the fiber cells lose their organelles (e.g., nuclei, mitochondria, endoplasmic reticulum [ER]), to form an organelle-free zone (OFZ) in the nuclear region.[2,3] Lenses of 1-month-old βA3ΔG91 mice exhibited attenuation of nuclei in the OFZ region relative to WT lenses during hematoxylin and eosin (H&E) staining and the presence of extensive vacuoles in the outer and inner cortex (Figs. 3A, 3B). The DAPI staining further confirmed the attenuation of nuclei in the OFZ region (Figs. 3C, 3D). IHC analysis of lens sections used anti-HSPA5 antibody (heat shock protein family A member 5, an Endoplasmic Reticulum chaperone that localizes in its lumen, and is involved in the folding and assembly of proteins). At 1 month of age, immunostaining of the ER with HSPA5 antibody was diminished in βA3ΔG91 lenses relative to WT lenses, suggesting a loss of ER in the mutant lenses (Figs. 3E, 3F). Together, the results suggest that the degradation of nuclei was impaired in the OFZ zone. In contrast, the ER levels were reduced in the same region, possibly due to the usage of the ER membranes in autophagosome formation during autophagy.[36–38]

The above result of the attenuation of nuclei degradation in βA3ΔG91 lenses relative to WT lenses was further corroborated by TEM analyses of the different regions of the lens (Fig. 4). In the lens epithelium, the mitochon-

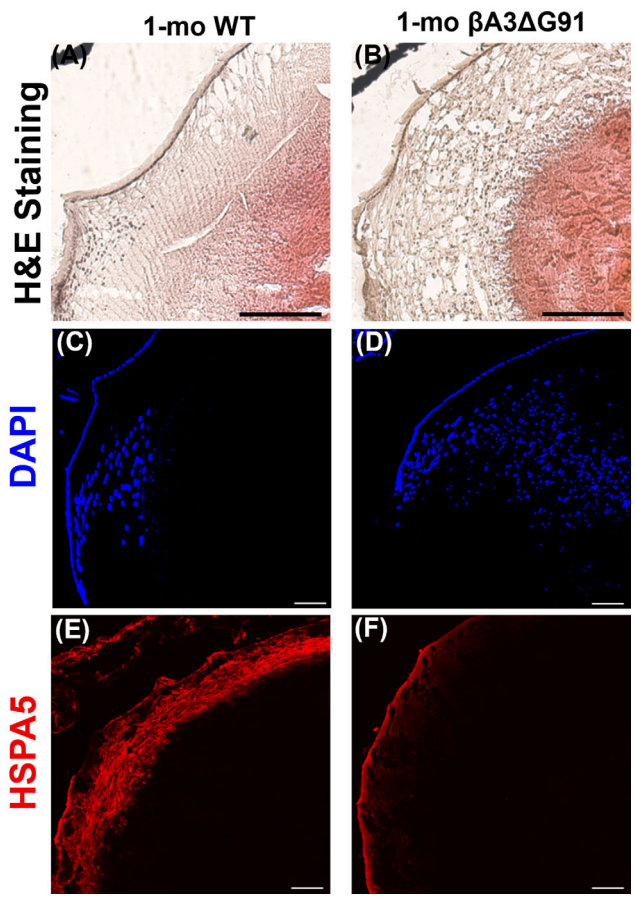

Figure 3. Impaired nuclei degradation in βA3ΔG91 relative to WT lenses. (**A**, **B**) H&E staining of WT and βA3ΔG91 lenses revealed the presence of several nuclei scattered throughout the lens. *Scale bar*: 200 µm. (**C**–**F**) Immunofluorescence with DAPI and HSPA5. (**C**, **D**) βA3ΔG91 contained more nuclei scattered throughout the lens than the WT lens. (**E**, **F**) There was a decrease in HSPA5 intensity, even though the area covered by the signal was similar in both WT and βA3ΔG91 lenses.

dria (M) and ER were equally present in both WT lenses (Fig. 4A) and βA3ΔG91 lenses (Fig. 4B), but the epithelium of βA3ΔG91 lenses showed the presence of extensive vacuoles (Fig. 4B). These organelles were also found in the outer cortex of both WT and βA3ΔG91 lenses (Figs. 4C, 4D). However, fewer ER were detected in the βA3ΔG91 lenses (Fig. 4D) than in the WT lenses. Interestingly, mitochondria present in the WT lenses were mostly elongated, whereas the mutants contained a combination of both round and elongated mitochondria. The round mitochondria might represent their degenerative nature. In the inner cortex (Figs. 4E–4H), relatively more condensed nuclei (N) forming inclusion bodies, disrupted nuclear envelopes, and chromatin seepage through breaks in the nuclear envelope into the cytosol were observed in βA3ΔG91 lenses (Figs. 4F, 4H).[39,40] The inner cortex of WT lenses exhibited signs of mitochondrial degradation, including discontinuous double membrane and loss of cristae (Figs. 4E, 4G), whereas βA3ΔG91 had intact mitochondria (Figs. 4F, 4H). In the nuclear region, the βA3ΔG91 lenses (Fig. 4J) exhibited disorganization of fiber cells and membranes in the regions proximal to the opacity.

Impaired Autophagy in βA3ΔG91 Lenses Relative to WT Lenses

Broadly, the four major sequential steps of autophagy are as follows: (1) After induction by a stress signal (e.g., starvation, oxidative stress, toxins), ubiquitination of proteins occurs. (2) p62, a cargo receptor for autophagy, binds to ubiquitinated proteins. (3) Autophagosome formation is initiated, and, concomitantly, a cytosolic form of LC3 (LC3-I, a 17-kDa microtubule-associated soluble protein 1A/1B light chain) is conjugated to phosphatidylethanolamine to form a LC3–phosphatidylethanolamine conjugate (LC3-II), which is recruited to autophagosomal membranes. (4) Autophagosome fusion with lysosomal constituents (e.g., lysosomal membrane proteins and enzymes) to form the autolysosome; during autophagy, autophagosomes engulf and degrade cytoplasmic components, including cytosolic proteins and organelles.[41] To examine whether autophagy might be linked to the attenuation of nuclei degradation in βA3ΔG91 lenses relative to WT lenses, we determined the expression of autophagy markers at both the transcriptional and translational levels during the specific autophagic steps described above.

Differential Expression of Autophagy Markers With Cataract Progression in βA3ΔG91 Mice

We examined mice lenses of βA3ΔG91 and WT mice at P0, P15, and P30 (1 month) for progressive cataract development and expression of an early autophagy marker. As expected, in contrast to clear lenses of WT mice, βA3ΔG91 mice exhibited a bilateral nuclear cataract at P0 (Fig. 5B) that progressively increased in size at P15 (Fig. 5D) and P30 (Fig. 5F) and showed microphakia. The lenses of the two types of mice at identical ages (i.e., at P0, P15, and P30) were also examined by IHC for the expression of p62 as an early autophagy marker. The expression of p62 at P0 was relatively elevated and scattered as puncta throughout both outer and inner cortical and nuclear regions in βA3ΔG91 lenses (Fig. 5H) relative to a lower expression in the WT lenses (Fig. 5G). In the P15 lenses, a greater level of immunoreactive proteins with anti-p62 antibody was observed which were mostly confined in the inner cortical and nuclear regions of the βA3ΔG91 lenses relative to WT lenses (Figs. 5I, 5J). The elevated p62 immunoreactivity throughout the lens at P0 in βA3ΔG91 lenses suggests that the autophagy process occurs in both epithelial and fiber cells during early differentiation but is disrupted relative to WT lenses. The disruption of autophagy is further supported by Figures 3 and 4, which show the attenuation of nuclei and mitochondrial degradation in βA3ΔG91 lenses relative to WT lenses. The elevated expression pattern of p62 in βA3ΔG91 was not surprising, because at P0 epithelial-to-fiber cell differentiation occurs throughout the lens; therefore, elevated p62 was observed in both cortical and nuclear regions. However, at the P15 and P30 stage, an active autophagic process to degrade organelles occurs in the outer and inner cortical regions to generate an OFZ, so its disruption is represented by elevated p62 in the cortical regions. The above results show that disruption of the autophagy process is an ongoing early event during epithelial-to-fiber cell differentiation along with early opacity development. Apparently, autophagosomes are also formed and fuse with the opaque region

Investigative Ophthalmology & Visual Science

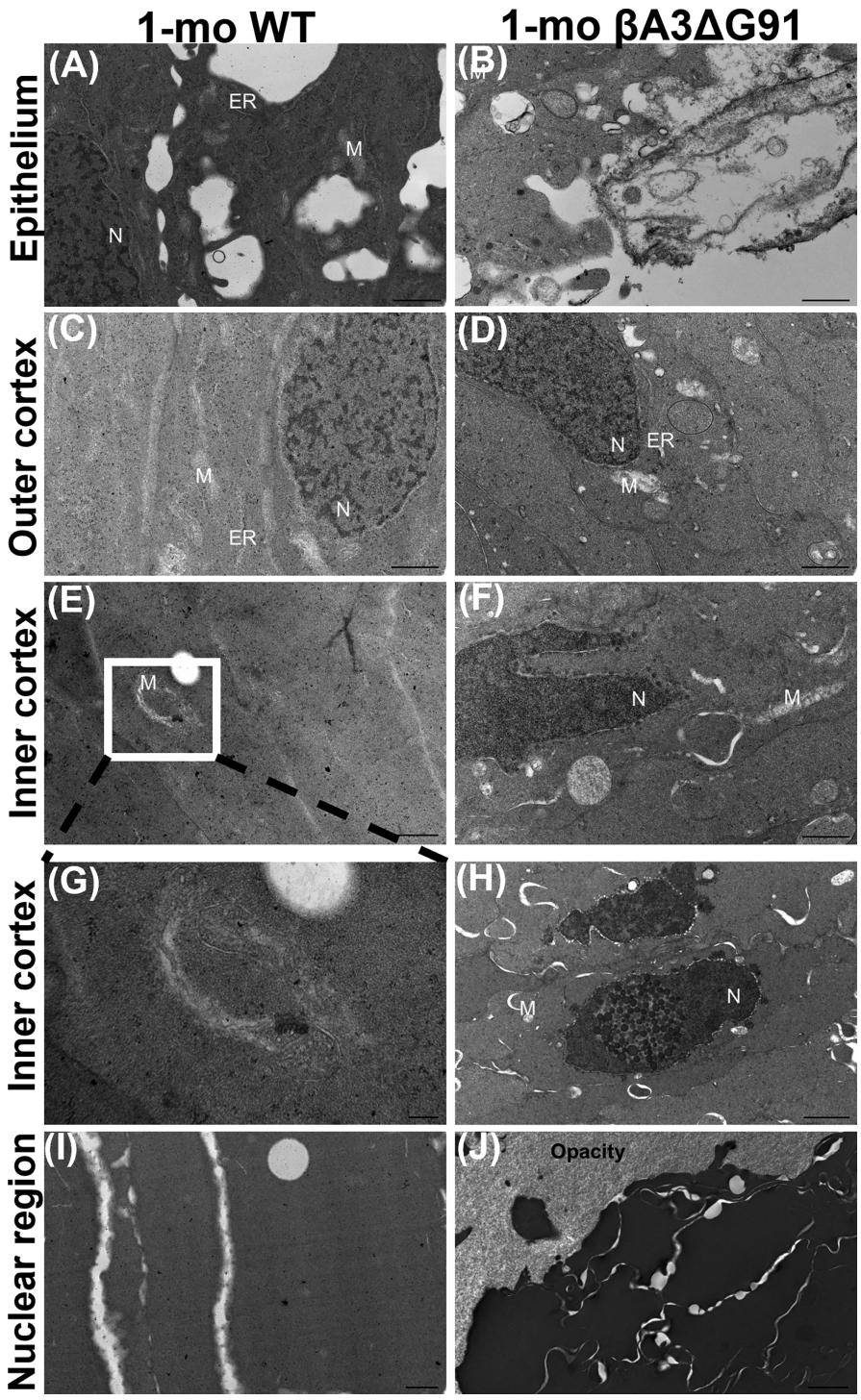

Figure 4. TEM analysis showing attenuation of nuclei and mitochondrial degradation in lenses of βA3ΔG91 mice relative to WT mice. (**A**, **B**) Epithelium, nuclei, ER, and mitochondria were present in both types of lenses. *Scale bar*: 1 µm. (**C**, **D**) In the outer cortex, less ER was spotted in the βA3ΔG91 than in the WT lens. *Scale bar*: 1 µm. (**E–H**) In the inner cortex, the βA3ΔG91 nuclear envelope was broken at some ends and chromatin exited into the cytosol. Some nuclear materials were packaged into inclusion bodies, forming a beaded appearance. The WT lens began to show mitochondria degradation. No ER was seen in either type of lens. *Scale bar*: 1 µm; inset, 400 nm. (**I**, **J**) In the nuclear region, adjacent fiber cells surrounding the region of opacity in βA3ΔG91 were highly disorganized. The WT lens was free of organelles or any opacity. *Scale bar*: 1 µm.

as supported by our TEM results in lenses of 1-month-old βA3ΔG91 mice (Figs. 8H, 8I). This led to our hypothesis that the opacity development might involve non-degradation of autophagosomes containing intact organelles, which might be due to lack of vacuolar (V)-ATPase activity to acidify lysosomes by the mutated βA3/A1-crystallin. Such lysosomal acidification is a normal process of the native βA3-crystallin.

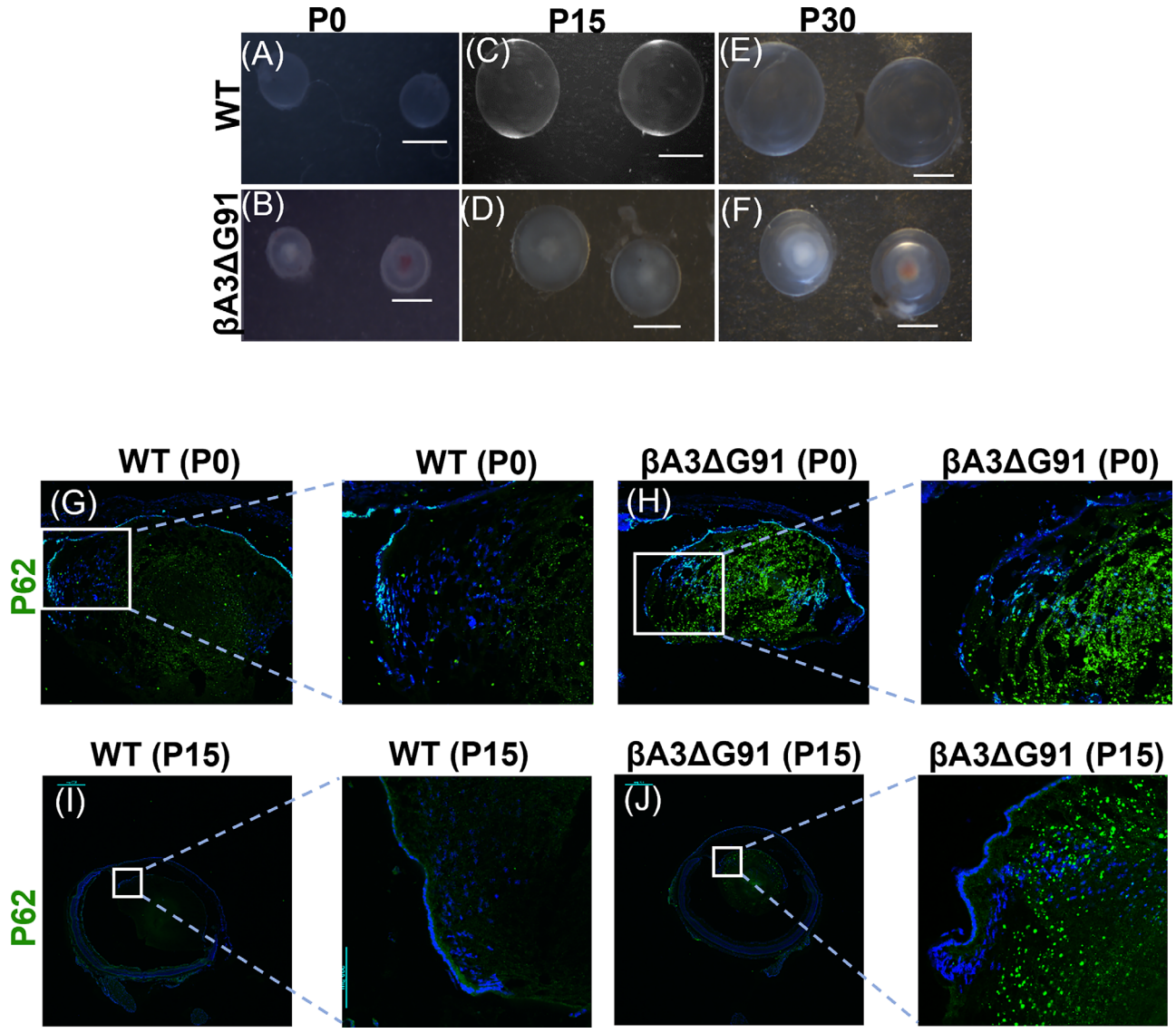

Figure 5. Differential expression of autophagy marker, p62, with cataract progression at P0, P15, and P30 (1 month) in βA3ΔG91 and WT mice. (**A–F**) Images of WT and βA3ΔG91 lenses at P0, P15, and P30. The lenses showed cataract development only in βA3ΔG91 mice at P0 which progressed in size at P15 and P30. (**G**, **H**) IHC analysis using anti-p62 antibody of lenses from WT and βA3ΔG91 mice at P0. (**I**, **J**) IHC analysis using anti-p62 antibody of lenses from WT and βA3ΔG91 mice at P15. Note the elevated levels of p62 immunoreactivity in the βA3ΔG91 lenses relative to the WT lenses.

Ubiquitination of Proteins and p62 Upregulation in βA3ΔG91 Lenses

One hallmark of the beginning of the autophagic process in a cell is the ubiquitination of proteins. Ubiquitin binds to misfolded proteins or superfluous organelles and tags them for degradation. In cases where autophagy is impaired, ubiquitin and p62 accumulate within cells.[42] On the other hand, p62 is an autophagy receptor that recognizes and binds to polyubiquitinated proteins to activate autophagy through its interaction with LC3.[43] To confirm whether aberrant organelle degradation in βA3ΔG91 lenses relative to WT lenses occurred due to impaired autophagy, these lenses were first examined for the presence of ubiquitinated proteins. IHC analyses showed that ubiquitin immunostaining was about three times greater in the βA3ΔG91 lenses relative to the WT lenses (Figs. 6A, 6B). Similarly, p62 puncta, which were mostly localized to the outer cortex, were also at relatively higher levels in βA3ΔG91 lenses (Figs. 6E, 6F) than the WT lenses (Figs. 6C, 6D). Additionally, p62 was localized at relatively higher levels in both outer and inner cortex and also within the immunoreactive βA3 ring region (Figs. 1E, 6E, 6F). The expression of p62 was also examined in cultured LECs from both types of mice. Under normal serum conditions, p62 immunofluorescence was relatively about three times higher in βA3ΔG91 LECs (Fig. 6I) than in the WT LECs (Fig. 6G), suggesting that p62 is upregulated in the former LECs.[44] Upon treatment with bafilomycin A1 (100-nM), p62 immunostaining intensities were significantly higher than under the normal serum conditions in both types of cells, but their levels were comparable (Figs. 6H, 6J). This showed that the effect of bafilomycin A1 treatment was similar between WT and mutant LECs. This is because bafilomycin A1 has been shown to inhibit the later stages

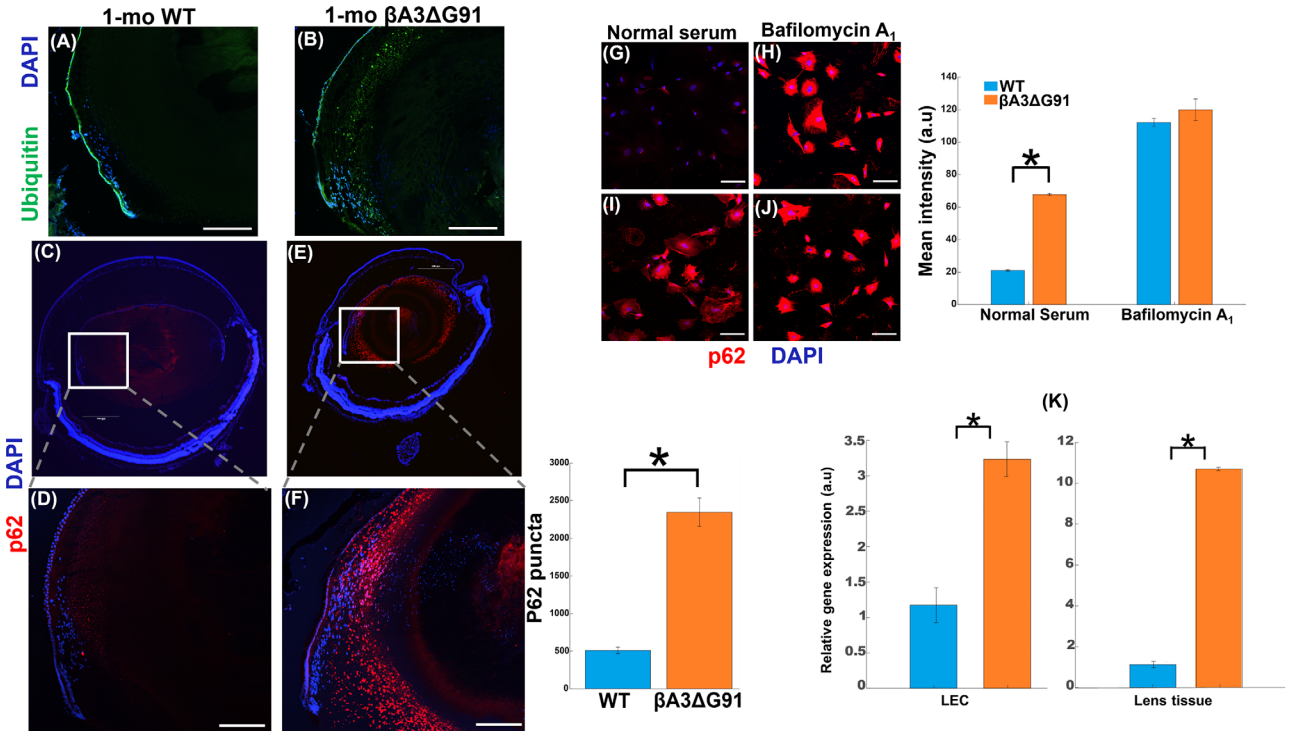

Figure 6. Ubiquitination of proteins and p62 upregulation in βA3ΔG91 relative to WT lenses. (**A**, **B**) Immunohistochemical analyses of ubiquitin in mouse lens sections. Ubiquitin expression was higher and seen as a band of speckles in the βA3ΔG91 relative to the WT lenses (10×). (**C–F**) Immunofluorescence analyses of p62 puncta demonstrated a significant increase in βA3ΔG91 relative to WT lenses (4×, 20×). *Scale bar*: 500 µm. (**G–J**) Immunofluorescence analyses of p62 in LECs showed increased p62 intensity in βA3ΔG91 LECs relative to WT under normal serum conditions. When cells were treated with bafilomycin A1, p62 was similarly upregulated in both WT and βA3ΔG91 LECs. *Scale bar*: 100 µm. *$P < 0.05$ versus age-matched WT. (**K**) p62 mRNA analyses showed 10-fold and threefold increases in p62 transcripts in βA3ΔG91 whole lenses and LECs, respectively.

of autophagy (inhibiting lysosomal acidification by inhibiting V-ATPase).[45] Additionally, when RT-qPCR quantified the levels of *p62* transcripts in both whole lens tissues and LECs, threefold and ninefold upregulation in the βA3ΔG91 relative to WT were observed in the LECs and lens tissues, respectively (Fig. 6K).

Elevated Levels of LC3 and LAMP2 Suggest Disruption of Autophagy

Labeling of LC3 serves as a way to track the binding of p62 and subsequent recruitment of autophagosomes and is therefore considered a good indicator of autophagosome formation. In cells, quantifying LC3-positive puncta is a gold-standard assay to assess autophagosome count.[46,47] Similarly, lysosome-associated membrane glycoprotein 2 (LAMP2) is a membrane glycoprotein that functions in the protection, maintenance, and adhesion of the lysosome.[48,49] To further expand our assessment that the accumulation of ubiquitin and p62 (Fig. 7) was due to impaired autophagosome formation or degradation by lysosomes, we examined the expression of LC3 and LAMP2 as markers for autophagosome and lysosome formation, respectively. LC3 exhibited a weak immunoreaction in the inner cortex but relatively strong staining in the nuclear region, forming a ring-like pattern in the βA3ΔG91 lens (Figs. 7D, 7F) relative to the WT lens (Figs. 7A, 7C). A similar pattern was seen with LAMP2 immunoreaction in βA3ΔG91 lenses relative to WT lenses, and LAMP2 was again colocalized in the ring-like structure (Figs. 7E, 7F). When LECs of βA3ΔG91 and WT lenses were cultured under normal serum conditions, the βA3ΔG91 LECs exhibited significantly higher immunofluorescence of LC3 and LAMP2 (Figs. 7J, 7K) relative to the LECs from normal lenses (Figs. 7G, 7H). Also, the evidence of relatively more yellow puncta in βA3ΔG91 (Fig. 7L) suggests the fusion of LC3 (autophagosomes) and LAMP2 (lysosomes) and a lack of autophagosome degradation. When the cells were grown under serum-starvation conditions to activate autophagy, LC3 and LAMP2 immunofluorescence intensities decreased in both groups of cells compared to normal serum conditions but were still relatively higher in the mutant LECs than the WT LECs (Figs. 7M, 7N, 7P, 7Q). The levels of LAMP2 and LC3 in LECs under normal serum and serum-starvation conditions were quantified as shown in bar graphs on the right side of the immune-stained LECs in Figure 7. The expression levels of LC3 and LAMP2 in lens tissues were also determined by RT-qPCR, which showed greater levels of LAMP2 in βA3ΔG91 lenses relative to WT lenses (Fig. 7V).

Another criterion used to assess autophagosome formation and degradation is the measurement of LC3-I to LC3-II conversion via western blot analysis. LC3-II is generated by the conjugation of cytosolic LC3-I to phosphatidylethanolamine (PE) to form LC3-II on the surface of nascent autophagosomes.[50] Results of the western blot analysis using 1-month-old lens homogenates showed that the ratio of LC3-II to LC3-I was higher in the mutant lenses

Investigative Ophthalmology & Visual Science

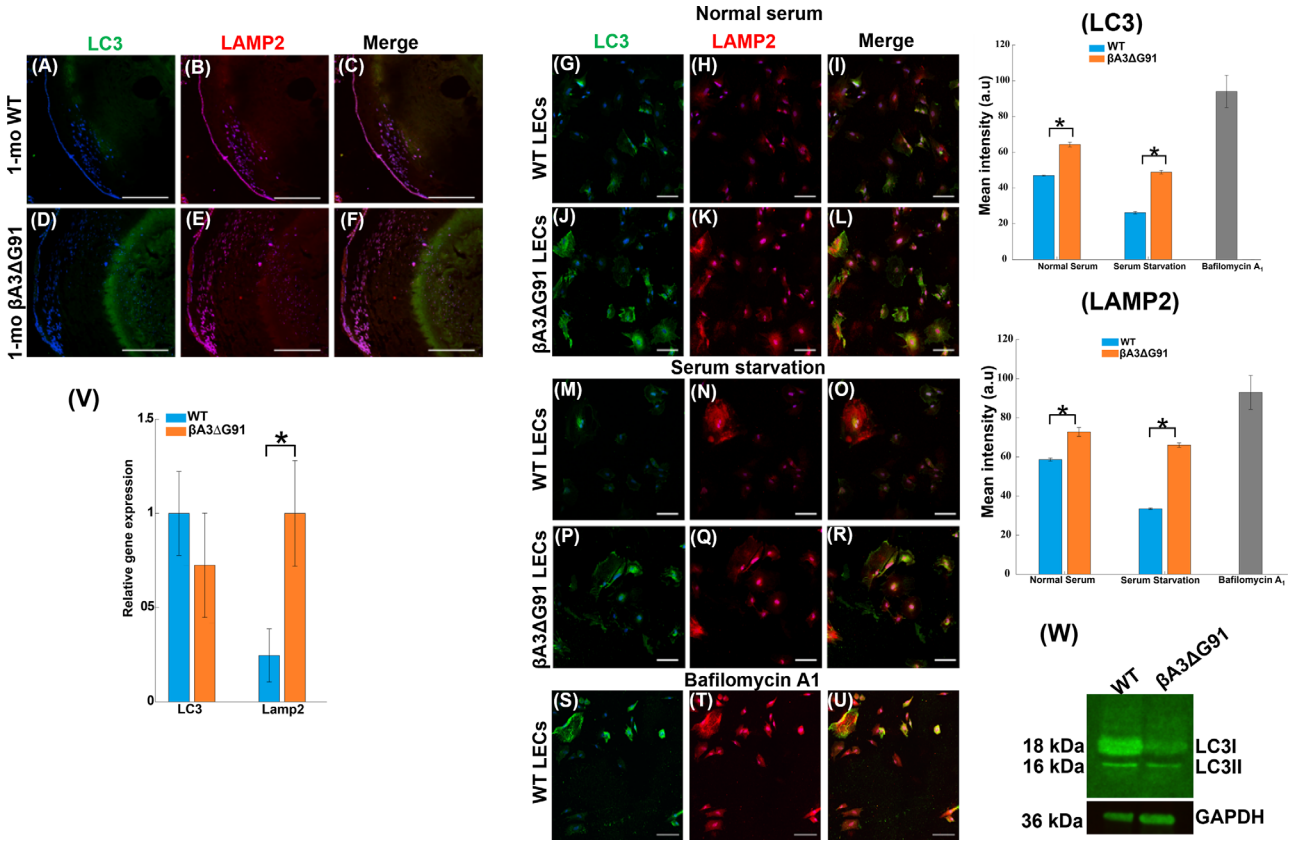

Figure 7. Elevated levels of LC3 and LAMP2 in βA3ΔG91 relative to WT lenses suggest disruption of autophagy. (**A–F**) Immunohistochemical analyses of LC3 and LAMP2 in mouse lens sections. LC3 and LAMP2 staining was higher in the βA3ΔG91 lenses than in the WT lenses (20×). (**G–L**) Under normal serum conditions, βA3ΔG91 LECs had higher LC3 and LAMP2 staining intensities relative to WT LECs. Yellow fluorescence in βA3ΔG91 indicated the presence of more undigested autolysosomes. (**M–R**) When cells were starved of serum, LC3 and LAMP2 were generally higher in the βA3ΔG91 LECs relative to the WT LECs. (**S–U**) When WT LECs were treated with bafilomycin A1, LC3 and LAMP2 immuno-intensities increased. *Scale bar*: 100 µm. (**V**) RT-qPCR analyses showed increased LAMP2 mRNA in the βA3ΔG91 lenses. *$P < 0.05$ versus age-matched WT. (**W**) Western blot analyses with anti-LC3 antibody showed a higher ratio of LC3-II to LC3-I in βA3ΔG91 relative to WT lenses.

compared to the WT lenses, suggesting normal formation but impeded breakdown of autophagosomes (Fig. 7W).

Autophagic Vesicles Accumulate in βA3ΔG91 Lenses

The above results showed that autophagy markers were relatively elevated, suggesting impaired autophagy in βA3ΔG91 lenses relative to WT lenses, but further structural assessment of autophagy was carried out by examining the presence of double-membrane autophagic vesicles by TEM analysis. In this study, we comparatively examined by TEM the cortex and nuclear regions of βA3ΔG91 and WT lenses for the presence of vacuoles, autophagosomes, and autolysosomes. Relative to the WT lens epithelium (Fig. 8A), the βA3ΔG91 lens epithelium exhibited several vesicles with double and single membranes (Figs. 8B, 8C, red arrows), representing autophagosomes and autolysosomes, respectively, and also large numbers of vacuoles. These vesicles seem to contain either cytoplasmic materials or cellular debris, which were absent in the WT epithelial cells. Double-membrane autophagic vesicles are characteristic of autophagosomes and single-walled vesicles result from the fusion of autophagosomes to lysosomes to form autolysosomes. In the cortex of βA3ΔG91 lenses, the accumulation of autophagic vesicles was observed (Fig. 8E, red arrows), but just a few virtually empty vesicles were seen in the cortex of WT lenses (Fig. 8D). The large vesicles in the βA3ΔG91 lens contained heterochromatin, membrane whorls, undegraded organelles, and double membrane-bound structures (Fig. 8F). A lysosome was observed lying at the boundary of the vesicle (Fig. 8F, white arrow). Interestingly, the βA3ΔG91 nuclei were condensed and formed inclusion/apoptotic bodies (Fig. 8E, circular dashes),[39] along with disrupted nuclear envelopes and chromatin seepage (Fig. 8E, white arrow). The nuclear region of βA3ΔG91 lenses contained several double-membrane vesicles (autophagosomes) and inclusion bodies that possibly fused with the nuclear opaque (cataract) region (Figs. 8H, 8I) but were absent in the same region of WT lenses (Fig. 8G). In summary, the findings of the comparative analyses of the elevated autophagic markers and double-membraned vesicles suggest that autophagy was disrupted in the βA3ΔG91 lenses relative to WT lenses.

Dysregulation of Autophagy Triggers Apoptosis in βA3ΔG91 Lenses

Our qPCR analyses showed that, relative to WT lenses, the βA3ΔG91 lenses exhibited downregulation of B-cell lymphoma 2 (Bcl-2; results not shown) and the presence

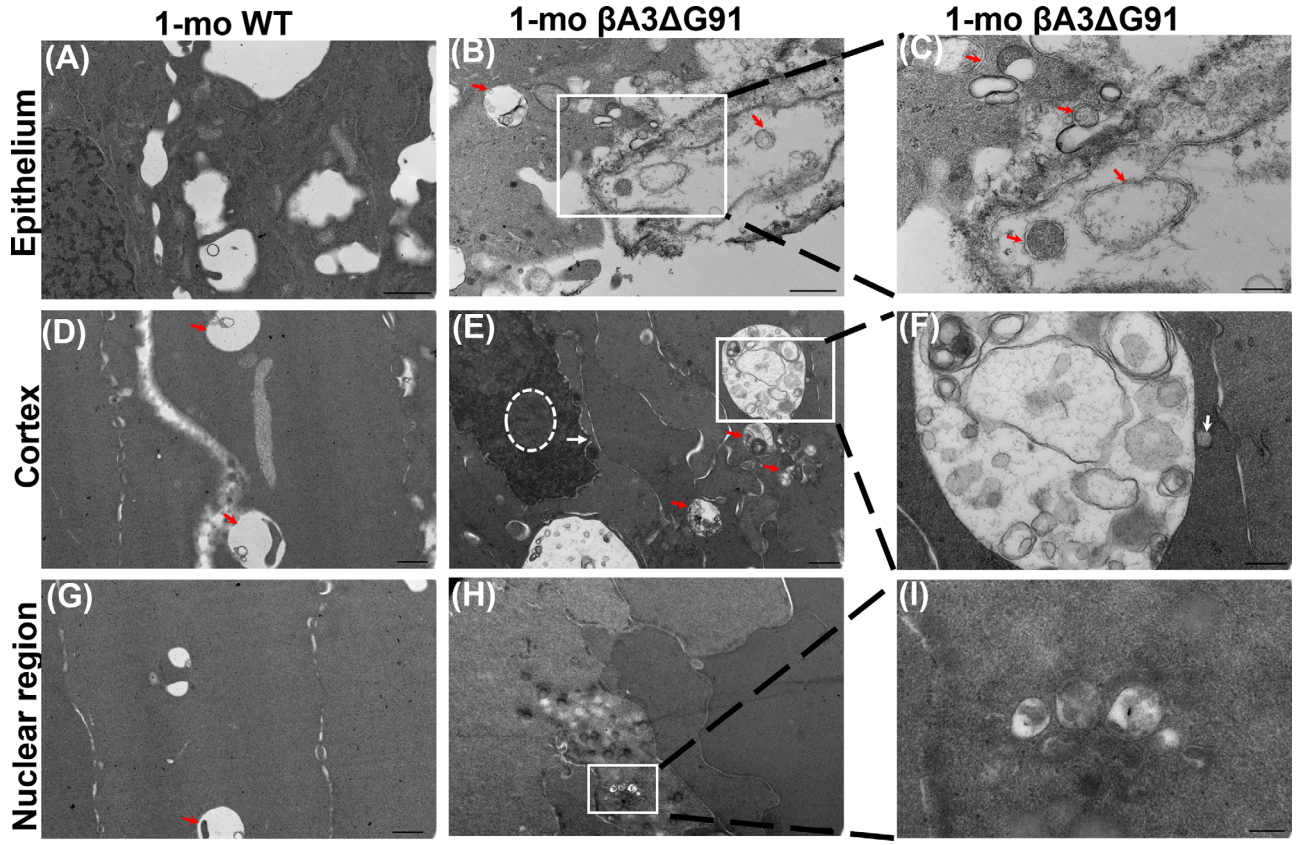

Figure 8. TEM analyses showed accumulation of autophagic vesicles in βA3ΔG91 versus WT lenses. (**A–C**) Several autophagosomes and autolysosomes were observed in the epithelium of βA3ΔG91 lenses compared to WT lenses. *Scale bar*: 1 µm. (**D–F**) Several autophagic vesicles containing cytoplasmic materials, membrane whorls, and heterochromatin were seen in the cortex of βA3ΔG91 but not WT lenses. *Scale bar*: 1 µm; inset, 400 nm. (**G–I**) Nuclear remnants and autophagic vesicles fused with the opaque (cataract) region in βA3ΔG91 lenses. *Scale bar*: 1 µm; inset, 200 nm. *Red arrows* indicate autophagosomes or autolysosomes. The *white arrow* points to a lysosome attached to an autophagosome.

of inclusion/apoptotic bodies, which suggested the possibility of apoptosis in the mutant lenses. Bcl-2 has been shown to be an anti-apoptotic protein that plays a role in regulating cell survival.[51] Additionally, impaired nuclei degradation in the lens can also cause unwanted organelles to build up and become toxic to the lens cells, which could also trigger apoptosis. During apoptosis, the release of activated caspases occurs. Therefore, we carried out a TUNEL assay and determined the levels of cleaved caspase-3 and caspase-9 in the two types of lenses. TUNEL staining of 1-month-old lenses showed more than three times higher apoptotic cells in the outer cortex and the nuclear region in βA3ΔG91 lenses compared to the WT lenses (Figs. 9A, 9B). This finding was supported by elevated levels of cleaved caspase-3 and caspase-9 in the LECs (Figs. 9D, 9E, 9G, 9H) and lens tissues (Figs. 9J, 9K, 9M, 9N) of βA3ΔG91 lenses relative to WT lenses.

Discussion

The focus of this study was to determine whether the delayed nuclei degradation in lenses of βA3ΔG91 mice relative to WT mice is associated with autophagy disruption, and if the disruption is evidenced by the relatively elevated levels of autophagy markers and the presence of double-membrane autophagosomes in βA3ΔG91 lenses. The rationale for the study was as follows. Our previous studies of both the complete βA3/A1-crystallin knockout mouse (βA3KO) model[33] and lens-specific βA3/A1 knockout mouse model (βA3cKO)[52] exhibited accumulation of undegraded organelles in the cortex and autophagy disruption. Also, βA3/A1-crystallin has been reported to be a retinal lysosomal resident protein in astrocytes, RPE cells, and ganglion cells,[30–32] and it modulates a specific autophagic-signaling pathway via V-ATPase.[31] Together, these findings suggest that βA3/A1-crystallin and V-ATPase proton pump interaction plays an essential role in regulating and maintaining lysosomal acidic pH. Based on the retinal reports, we have hypothesized that βA3/A1-crystallin acts similarly in the lens, and either its absence in βA3KO and βA3cKO lenses or its dysfunction due to G91-deletion in lenses would disrupt the autophagy process. As stated above, the dysfunctional nature of βA3ΔG91 is supported by in vitro studies of the recombinant βA3ΔG91, showing its altered structure, precipitation, and inability to oligomerize with other crystallins.[19,35] More importantly, G91Del in βA3/A1-crystallin resulted in congenital cataract development among families in various countries.[13–19]

The reason for the dysfunctional βA3ΔG91 in vivo is that G91 is located at a conserved key site that stabilizes the structures of both β- and γ-crystallins (members of a super family). Both crystallins contain two similar consecu-

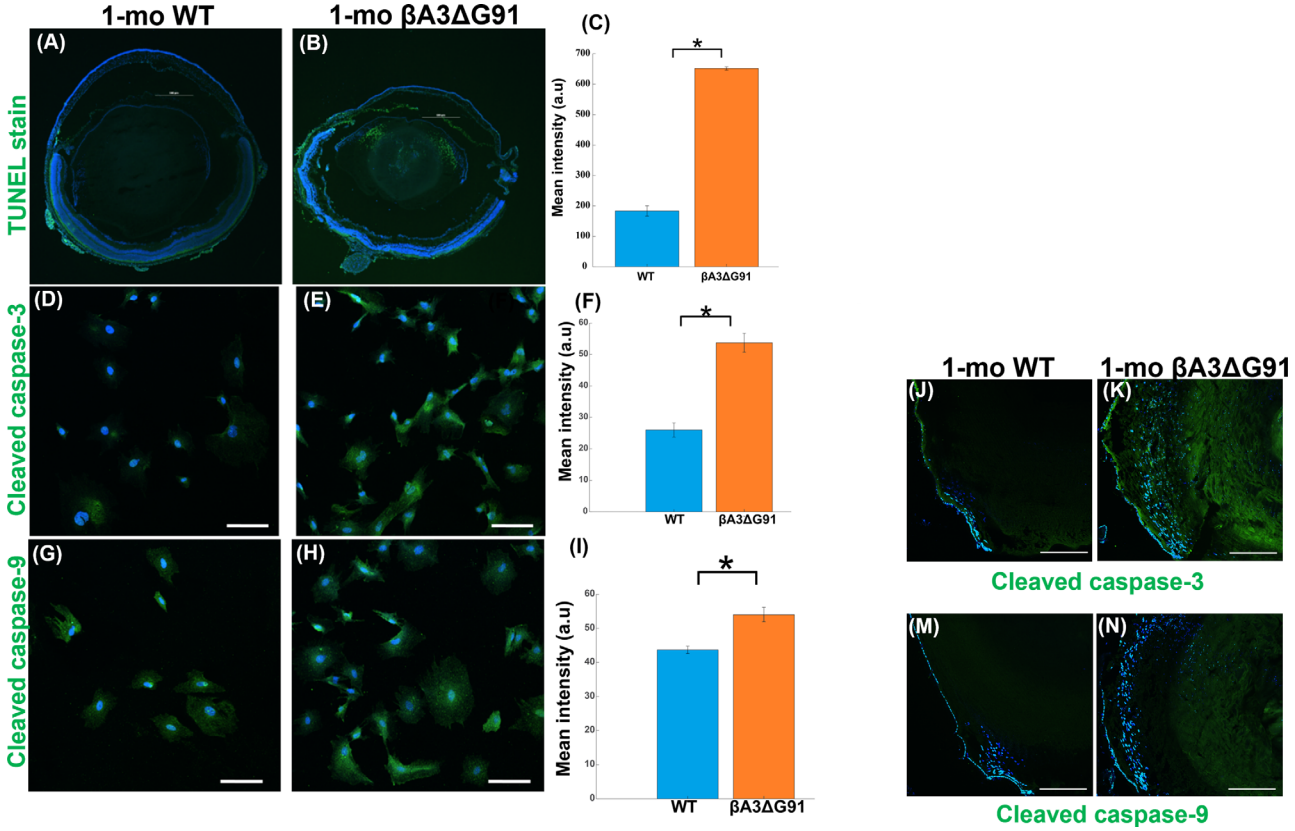

Figure 9. Dysregulation of autophagy triggers apoptosis in βA3ΔG91 lenses. (**A–C**) TUNEL stain. Several TUNEL-positive cells appear as puncta, co-localizing with nuclei in βA3ΔG91 relative to WT lenses (4×). *Scale bar*: 500 µm. (**D–F**) Expression of cleaved caspase-3 was higher in βA3ΔG91 relative to WT LECs. (**G–I**) Expression of cleaved caspase-9 was higher in βA3ΔG91 relative to WT LECs. $^{*}P < 0.05$ versus age-matched WT. (**J**, **K**) Relative immunofluorescence signal demonstrated a notable increase in cleaved caspase-3 expression in the βA3ΔG91 lenses compared to the WT lenses. (**M**, **N**) Higher immunofluorescence intensity for cleaved caspase-9 in the βA3ΔG91 relative to the WT lenses.

tive N-terminal domains with Greek key motifs 1 and 2. Similarly, the C-terminal domain contains Greek key motifs 3 and 4.[19,53,54] Each Greek key motif is comprised of four consecutive β strands (a–d) that intercalate to form two β sheets.[19] The G91 deletion in βA3-crystallin results in the loss of G91 at the edge of strand c in the second motif of the N-terminal domain, affecting the conserved structural feature known as the tyrosine corner. This tyrosine corner is known to stabilize the connection between b and c β strands and is present in most β-sandwich domains, where they appear to stabilize the fold topology in β- and γ-crystallins.[53,54] Therefore, G91 deletion leads to major structural destabilization rendering a dysfunctional βA3-crystallin, as evidenced by the results of recombinant βA3-crystallin.[19,35]

βA3ΔG91 mice developed congenital nuclear cataract (Fig. 5B), which potentially results from (1) attenuation of nuclei and mitochondrial degradation in the lens inner cortex due to autophagy disruption, (2) cellular apoptosis, or (3) βA3ΔG91 insolubilization. Relative to WT lenses, the undegraded nuclei were seen in the OFZ of βA3ΔG91 lenses during nuclear staining by H&E and DAPI staining (Fig. 3) and during TEM analysis of lens sections (Fig. 4). Interestingly, the relative expression of HSPA5 (an ER marker) in βA3ΔG91 lenses was rather decreased, which could be indicative of an impaired protein quality control system. Evidence shows that, when autophagy is disrupted, there is a higher burden of misfolded proteins, which can overwhelm the protein folding and quality control machinery.[55] Because HSPA5 is a chaperone that facilitates the clearance of misfolded proteins, its decreased levels may indicate an inability to cope with the increased load of misfolded proteins, which may be linked to autophagy disruption.[55,56] The higher ubiquitination of proteins in βA3ΔG91 lenses relative to WT lenses provides further evidence for the increased levels of damaged/unfolded proteins in the mutant lenses.

Because past reports and our recent reports of βA3KO[33] and βA3cKO[52] mouse models have implicated the attenuation of lens organelle degradation in autophagy, this prompted us to investigate in this study the effects of dysfunctional βA3ΔG91 on autophagy in the lenses of βA3ΔG91 versus WT mice. The following relative results suggest autophagy disruption in the βA3ΔG91 lenses: (1) attenuation of nuclei and mitochondrial degradation (Figs. 3, 4), (2) elevated autophagy markers (Figs. 6–8), (3) accumulation of autophagosomes and autolysosomes with undigested organelles (Fig. 8), (4) activated cellular apoptosis (Fig. 9), and (5) βA3-crystallin insolubilization (Table 2).

βA3ΔG91 lenses showed relatively higher levels of ubiquitinated proteins (Fig. 6). The ubiquitination of target proteins (a posttranslational modification process) acts either as a signal for the substrates to be degraded by proteasome or lysosome or as an indicator for modulating their

non-proteolytic processes.[44] This is evidenced by reported crosstalk between autophagy and the ubiquitin-proteasome system.[57] Relative to WT lenses, p62 was upregulated at both transcriptional and translational levels in both βA3ΔG91 lenses and LECs (Figs. 6, 7). The increased levels of p62 are indicative of defective autophagic flux in various diseases, and p62 is also an autophagy substrate that is used as a reporter of autophagic activity.[43] Similarly, LC3-II levels were increased in βA3ΔG91 lenses relative to WT lenses (Fig. 7). LC3-II, a standard marker for autophagosomes, is generated by the conjugation of cytosolic LC3-I to PE on the surface of nascent autophagosomes.[46,47] As LC3 is specifically associated with autophagosomes and autolysosomes, quantifying LC3-positive puncta is considered a gold-standard assay for assessing the numbers of autophagosomes in cells.[46] LAMP2 was also relatively upregulated in βA3ΔG91 lenses and LECs (Fig. 7). LAMP1 and LAMP2 comprise 50% of all lysosomal membrane proteins, and are thought to be responsible in part for maintaining lysosomal integrity, pH, and catabolism. LAMP2 gene mutation causes lysosomal storage disease in humans.[46,49] In embryonic fibroblasts, disruption of both LAMP1 and LAMP2 is associated with Danon disease, including accumulation of autophagic vacuoles in heart and skeletal muscles.[58] Similar vacuoles were also observed in the epithelial cells of βA3ΔG91 lenses relative to those of WT cells (Fig. 8). The autophagosomes, large double-membrane vesicles enclosing cytoplasmic components that are targeted for degradation during autophagy, were also observed during TEM analysis of βA3ΔG91 lenses (Fig. 8). The double-membrane autophagosomes are the hallmark of the catabolic pathway during autophagy.[38] Interestingly, the TEM images in Figure 8 show the presence of autophagosomes in the epithelium, cortex, and nuclear region. One intriguing finding from TEM images was the fusion of autophagosomes with the nuclear opaque region, representing its potential role in cataract development. Currently, the identity of the autophagosomes that fuse with the opaque region is unknown, and whether the fusion plays a role in the nuclear opacity development in the βA3ΔG91 lenses is also unknown. This led to our hypothesis that the opacity development in βA3ΔG91 lenses is associated with non-degradation of autophagosomes which might be due to lack of V-ATPase activity to acidify lysosomes. Such lysosomal acidification is a normal process by the native βA3-crystallin in the retina.[31]

The lenses of βA3ΔG91 mice also exhibited activated apoptosis in the nuclear region relative to WT lenses. IHC analyses showed that cleaved caspase-3 and caspase-9 were relatively upregulated in the βA3ΔG91 LECs (Fig. 9). Apoptosis has been suggested as a decisive process for cell death during autophagy.[59] Because caspase-9 on activation cleaves caspase-3 and caspase-7, which are effector caspases that carry out apoptosis via DNA fragmentation, cell shrinkage, and membrane blebbing, it is difficult to determine the levels of the two caspases by western blot analysis. Therefore, the use of IHC is preferable to western blot analysis for determining the levels of caspase-3 and caspase-9.

In summary, the results from our study provide evidence that our novel mouse model shares a similar phenotype with βA3ΔG91 human patients. Similar to total and conditional *CRYβA1* knockout mice, βA3ΔG91 lenses showed impaired autophagy. Based on the association of βA3ΔG91 with autophagy dysregulation, further investigations are warranted to explore the potential role of *CRYβA1* as an autophagy regulator via the V-ATPase modulator in the lens.

Acknowledgments

The authors thank Lawrence Sincich, PhD, for helping with isolated lens imaging.

Supported by grants from the National Institutes of Health (EY031303, P30-EY03039).

Disclosure: **A.K. Boateng,** None; **R. Joseph,** None; **O.P. Srivastava,** None

References

1. Cvekl A, Ashery-Padan R. The cellular and molecular mechanisms of vertebrate lens development. *Development*. 2014;141:4432–4447.
2. Bassnett S. Lens organelle degradation. *Exp Eye Res*. 2002;74:1–6.
3. Brennan L, Disatham J, Kantorow M. Mechanisms of organelle elimination for lens development and differentiation. *Exp Eye Res*. 2021;209:108682.
4. Costello MJ, Brennan LA, Basu S, et al. Autophagy and mitophagy participate in ocular lens organelle degradation. *Exp Eye Res*. 2013;116:141–150.
5. Li H, Gao L, Du J, et al. Impacts of autophagy on the formation of organelle-free zone during the lens development. *Mol Biol Rep*. 2023;50:4551–4564.
6. Morishita H, Mizushima N. Autophagy in the lens. *Exp Eye Res*. 2016;144:22–28.
7. Chen J, Ma Z, Jiao X, et al. Mutations in *FYCO1* cause autosomal-recessive congenital cataracts. *Am J Hum Genet*. 2011;88:827–838.
8. Huang J, Yu W, He Q, et al. Autophagy facilitates age-related cell apoptosis-a new insight from senile cataract. *Cell Death Dis*. 2022;13:37.
9. Medsinge A, Nischal KK. Pediatric cataract: challenges and future directions. *Clin Ophthalmol*. 2015;9:77–90.
10. Holmes JM, Leske DA, Burke JP, Hodge DO. Birth prevalence of visually significant infantile cataract in a defined U.S. population. *Ophthalmic Epidemiol*. 2003;10:67–74.
11. Reddy MA, Francis PJ, Berry V, Bhattacharya SS, Moore AT. Molecular genetic basis of inherited cataract and associated phenotypes. *Surv Ophthalmol*. 2004;49:300–315.
12. Hejtmancik JF. Congenital cataracts and their molecular genetics. *Semin Cell Dev Biol*. 2008;19:134–149.
13. Ferrini W, Schorderet DF, Othenin-Girard P, Uffer S, Heon E, Munier FL. CRYBA3/A1 gene mutation associated with suture-sparing autosomal dominant congenital nuclear cataract: a novel phenotype. *Invest Ophthalmol Vis Sci*. 2004;45:1436–1441.
14. Gu Z, Ji B, Wan C, et al. A splice site mutation in *CRYBA1/A3* causing autosomal dominant posterior polar cataract in a Chinese pedigree. *Mol Vis*. 2010;16:154–160.
15. Kannabiran C, Rogan PK, Olmos L, et al. Autosomal dominant zonular cataract with sutural opacities is associated with a splice mutation in the βA3/A1-crystallin gene. *Mol Vis*. 1998;4:21.
16. Li D, Jing Q, Jiang Y. The identification and characterization of the p.G91 deletion in CRYBA1 in a Chinese family with congenital cataracts. *BMC Med Genet*. 2019;20:153.
17. Lu S, Zhao C, Jiao H, et al. Two Chinese families with pulverulent congenital cataracts and DG91 CRYBA1 mutations. *Mol Vis*. 2007;13:1154–1160.
18. Qi Y, Jia H, Huang S, et al. A deletion mutation in the βA3/A1 crystallin gene (CRYBA1/A3) is associated

with autosomal dominant congenital nuclear cataract in a Chinese family. *Hum Genet*. 2004;114:192–197.
19. Reddy MA, Bateman OA, Chakarova C, et al. Characterization of the G91del CRYBA1/3-crystallin protein: a cause of human inherited cataract. *Hum Mol Genet*. 2004;13:945–953.
20. Sun W, Xiao X, Li S, Guo X, Zhang Q. Mutation analysis of 12 genes in Chinese families with congenital cataracts. *Mol Vis*. 2011;17:2197.
21. Wang KJ, Zha X, Chen DD, Zhu SQ. Mutation analysis of families with autosomal dominant congenital cataract: a recurrent mutation in the *CRYBA1/A3* gene causing congenital nuclear cataract. *Curr Eye Res*. 2018;43:304–307.
22. Yang G, Zhai X, Zhao J. A recurrent mutation in CRYBA1 is associated with an autosomal dominant congenital nuclear cataract disease in a Chinese family. *Mol Vis*. 2011;17:1559.
23. Yang Z, Li Q, Ma Z, Guo Y, Zhu S, Ma X. AG→ T splice site mutation of *CRYBA1/A3* associated with autosomal dominant suture cataracts in a Chinese family. *Mol Vis*. 2011;17:2065.
24. Mohebi M, Akbari A, Babaei N, Sadeghi A, Heidari M. Identification of a de novo 3bp deletion in *CRYBA1/A3* gene in autosomal dominant congenital cataract. *Acta Med Iran*. 2016;54:778–783.
25. Berbers GA, Hoekman WA, Bloemendal H, de Jong WW, Kleinschmidt T, Braunitzer G. Homology between the primary structures of the major bovine β-crystallin chains. *Eur J Biochem*. 1984;139:467–479.
26. Herbrink P, Van Westreenen H, Bloemendal H. Further studies on the polypeptide chains of β-crystallin. *Exp Eye Res*. 1975;20:541–548.
27. Werten PJ, Stege GJ, de Jong WW. The short 5′ untranslated region of the βA3/A1-crystallin mRNA is responsible for leaky ribosomal scanning. *Mol Biol Rep*. 1999;26:201–205.
28. Blundell T, Lindley P, Miller L, et al. The molecular structure and stability of the eye lens: x-ray analysis of γ-crystallin II. *Nature*. 1981;289:771–777.
29. Parthasarathy G, Ma B, Zhang C, et al. Expression of βA3/A1-crystallin in the developing and adult rat eye. *J Mol Histol*. 2011;42:59–69.
30. Gehlbach P, Hose S, Lei B, et al. Developmental abnormalities in the Nuc1 rat retina: a spontaneous mutation that affects neuronal and vascular remodeling and retinal function. *Neuroscience*. 2006;137:447–461.
31. Valapala M, Wilson C, Hose S, et al. Lysosomal-mediated waste clearance in retinal pigment epithelial cells is regulated by CRYBA1/βA3/A1-crystallin via V-ATPase-MTORC1 signaling. *Autophagy*. 2014;10:480–496.
32. Zigler JS, Jr, Zhang C, Grebe R, et al. Mutation in the βA3/A1-crystallin gene impairs phagosome degradation in the retinal pigmented epithelium of the rat. *J Cell Sci*. 2011;124:523–531.
33. Hegde S, Kesterson RA, Srivastava OP. CRYβA3/A1-crystallin knockout develops nuclear cataract and causes impaired lysosomal cargo clearance and calpain activation. *PLoS One*. 2016;11:e0149027.
34. Valapala M, Hose S, Gongora C, et al. Impaired endolysosomal function disrupts Notch signalling in optic nerve astrocytes. *Nat Commun*. 2013;4:1–12.
35. Xu J, Wang H, Wu C, et al. Pathogenic mechanism of congenital cataract caused by the CRYBA1/A3-G91del variant and related intervention strategies. *Int J Biol Macromol*. 2021;189:44–52.
36. Yamamoto YH, Noda T. Autophagosome formation in relation to the endoplasmic reticulum. *J Biomed Sci*. 2020;27:97.
37. Li YN, Zhou Q, Yang B, et al. Mechanism of rat osteosarcoma cell apoptosis induced by a combination of low-intensity ultrasound and 5-aminolevulinic acid in vitro. *Genet Mol Res*. 2015;14:9604–9613.
38. Nakatogawa H. Mechanisms governing autophagosome biogenesis. *Nat Rev Mol Cell Biol*. 2020;21:439–458.
39. Costello MJ, Brennan LA, Mohamed A, Gilliland KO, Johnsen S, Kantorow M. Identification and ultrastructural characterization of a novel nuclear degradation complex in differentiating lens fiber cells. *PLoS One*. 2016;11:e0160785.
40. Tesoro S, Ali I, Morozov AN, Sulaiman N, Marenduzzo D. A one-dimensional statistical mechanics model for nucleosome positioning on genomic DNA. *Phys Biol*. 2016;13:016004.
41. Mizushima N. Autophagy: process and function. *Genes Dev*. 2007;21:2861–2873.
42. Yin Z, Popelka H, Lei Y, Yang Y, Klionsky DJ. The roles of ubiquitin in mediating autophagy. *Cells*. 2020;9:2025.
43. Pankiv S, Clausen TH, Lamark T, et al. p62/SQSTM1 binds directly to Atg8/LC3 to facilitate degradation of ubiquitinated protein aggregates by autophagy. *J Biol Chem*. 2007;282:24131–24145.
44. Shaid S, Brandts CH, Serve H, Dikic I. Ubiquitination and selective autophagy. *Cell Death Differ*. 2013;20:21–30.
45. Zhang J, Feng Y, Forgac M. Proton conduction and bafilomycin binding by the V0 domain of the coated vesicle V-ATPase. *J Biol Chem*. 1994;269:23518–23523.
46. Runwal G, Stamatakou E, Siddiqi FH, Puri C, Zhu Y, Rubinsztein DC. LC3-positive structures are prominent in autophagy-deficient cells. *Sci Rep*. 2019;9:10147.
47. Klionsky DJ, Abdel-Aziz AK, Abdelfatah S, et al. Guidelines for the use and interpretation of assays for monitoring autophagy (4th edition). *Autophagy*. 2021;17:1–382.
48. Terasawa K, Tomabechi Y, Ikeda M, et al. Lysosome-associated membrane proteins-1 and -2 (LAMP-1 and LAMP-2) assemble via distinct modes. *Biochem Biophys Res Commun*. 2016;479:489–495.
49. Eskelinen EL. Roles of LAMP-1 and LAMP-2 in lysosome biogenesis and autophagy. *Mol Aspects Med*. 2006;27:495–502.
50. Mizushima N, Yoshimori T. How to interpret LC3 immunoblotting. *Autophagy*. 2007;3:542–545.
51. Tzifi F, Economopoulou C, Gourgiotis D, Ardavanis A, Papageorgiou S, Scorilas A. The role of BCL2 family of apoptosis regulator proteins in acute and chronic leukemias. *Adv Hematol*. 2012;2012:524308.
52. Joseph R, Robinson ML, Lambert L, Srivastava OP. Lens-specific βA3/A1-conditional knockout mice: phenotypic characteristics and calpain activation causing protein degradation and insolubilization. *PLoS One*. 2023;18:e0281386.
53. Basak A, Bateman O, Slingsby C, et al. High-resolution X-ray crystal structures of human gammaD crystallin (1.25 A) and the R58H mutant (1.15 A) associated with aculeiform cataract. *J Mol Biol*. 2003;328:1137–1147.
54. Hemmingsen JM, Gernert KM, Richardson JS, Richardson DC. The tyrosine corner: a feature of most Greek key β-barrel proteins. *Protein Sci*. 1994;3:1927–1937.
55. Li J, Ni M, Lee B, Barron E, Hinton DR, Lee AS. The unfolded protein response regulator GRP78/BiP is required for endoplasmic reticulum integrity and stress-induced autophagy in mammalian cells. *Cell Death Differ*. 2008;15:1460–1471.
56. Kim SY, Kim HJ, Kim HJ, et al. HSPA5 negatively regulates lysosomal activity through ubiquitination of MUL1 in head and neck cancer. *Autophagy*. 2018;14:385–403.
57. Kocaturk NM, Gozuacik D. Crosstalk between mammalian autophagy and the ubiquitin-proteasome system. *Front Cell Dev Biol*. 2018;6:128.

Investigative Ophthalmology & Visual Science

58. Choi SI, Dadakhujaev S, Maeng YS, Ahn SY, Kim TI, Kim EK. Disrupted cell cycle arrest and reduced proliferation in corneal fibroblasts from GCD2 patients: a potential role for altered autophagy flux. *Biochem Biophys Res Commun*. 2015;456:288–293.

59. Liu J, Copland DA, Theodoropoulou S, et al. Impairing autophagy in retinal pigment epithelium leads to inflammasome activation and enhanced macrophage-mediated angiogenesis. *Sci Rep*. 2016;6:20639.

Investigative Ophthalmology & Visual Science